Membrane and Water Treatment, *Vol. 17, No. 1 (2026) 1-19*
https://doi.org/10.12989/mwt.2026.17.1.001

Techno-Press

Heat and mass transfer correlations and fouling in air gap membrane distillation of benzene–water

Divya Gaur, Sushant Upadhyaya*, Kailash Singh, Rajeshwar Kholapure

Department of Chemical Engineering, Malaviya National Institute of Technology, Jaipur – 302017, India

(Received March 13, 2024, Revised September 9, 2025, Accepted December 30, 2025)

Abstract. This study focused on the separation of a benzene-water mixture using the air gap membrane distillation. The hydrophobic microporous membrane made up of poly-tetrafluoroethylene of 0.22 micron average pore size was used in the membrane module of the air gap membrane distillation experimental setup. The heat transfer and mass transfer correlations have been developed. It was found that the heat transfer and mass transfer coefficient increases from 523.27 to 1786.36 W/m^{2}K, and 1.08 $\times 10^{-1}$ to 1.99$\times 10^{-1}$ cm/s, respectively, on increasing the feed bulk inlet temperature from 40 to 60°C at a feed flow rate of 5 lpm under a 3 mm air gap in the membrane module. The effect of fouling phenomena on permeate flux and membrane characteristics was also investigated, and it was found that the permeate flux decreased from 6.50 kg/m^{2}h to 6.38 kg/m^{2}h under 420 hr. This clearly shows that negligible fouling was encountered on the membrane surface during continuous usage of the air gap membrane distillation setup. The membrane before and after 420 hr was characterized quantitatively and qualitatively using atomic force microscopy and field emission scanning electron microscope. The average pore size for the new membrane, used membrane after 420 hr and water wash membrane was analyzed using Image J software. Pore Size Distribution is plotted which confirms that the membrane characteristics were not affected to an extent. This clearly shows the stand alone capability of air gap membrane distillation process for separation of organic compounds from aqueous solution.

Keywords: air gap membrane distillation; FE-SEM and AFM; heat and mass transfer correlation; poly-tetra-fluoro-ethylene

1. Introduction

Water scarcity is a critical issue that affects millions of people worldwide. Lack of access to clean and safe water is a major challenge, particularly in developing nations. Population growth, climate change, and the irresponsible use of water resources have all contributed to this issue [1]. Water scarcity impacts agriculture, industry, and the environment in addition to human health and well-being [2-4]. It is essential to implement sustainable water management practices and invest in technologies to mitigate the negative effects of water scarcity. Among the most widespread organic pollutants, volatile organic compounds are distinguished. Generally, they inhabit effluent as well as natural aquatic environment [5]. After a year of monitoring these volatile organic compounds in surface and purified water, Ramos et al. [6] determined that they posed significant hazards to human well-being and to the environment. Volatile Organic Compounds are released

*Corresponding author, Associate Professor, E-mail: supadhyay.chem@mnit.ac.in

http://www.techno-press.org/mwt/5

ISSN: 2005-8624 (Print), 2092-7037 (Online)

into the aquatic ecosystem through natural degradation, agricultural practices, and industrial effluent discharges, including those from rubber processing, plastics, pulp and paper mills as well as paint shops, oil refineries, resin manufacturing, and cellulose, dyes, textile, tannery, pharmaceutical, and petroleum. They are among the US Environmental Protection Agency's (EPA) priority pollutants due to their unpleasant flavor, foul smell, and cytotoxicity even at low concentrations. Therefore, eradicating them from natural water becomes the utmost significance [7].

Volatile Organic Compounds have recently been the subject of extensive research and have become a major public concern. Volatile Organic Compounds includes aromatics compounds, alcohols, ketones, alkanes, esters, and secondary organic harmful substances. The process of eliminating of volatile organic compounds from water is challenging due to their stability and solubility. Numerous compounds have low solubility in water and modest acidity, but high solubility in organic solvents. To guarantee a secure water supply, it is essential to come up with efficient methods for removing these compounds. The strategies used in conventional methods can have a number of drawbacks, including insufficient treatment, process instability. For instance, the chlorination phase utilized in water disinfection can result in the formation of by-products that are more hazardous to humans and the environment than their precursors. Several techniques for controlling have been created and implemented to eliminate volatile organic compounds, which include plasma technology, adsorption, absorption, bio-filtration, membrane filtration, incineration, and condensation [8]. Among membrane technologies, membrane distillation (MD) is highlighted as a viable alternative because it can be adapted to treat a variety of complex water matrices under various conditions Ezugbe and Rathilal [9]. The MD driving force is the temperature gradient, which induces vapor transport through the membrane pores by generating a water vapor pressure differential. Typically, 30°C temperature gradient is adequate to facilitate separation [4].

Similarly, when compared to the traditional distillation process and other membrane technologies such as nanofiltration, reverse osmosis, and electrodialysis, the MD has certain advantages: (a) low operating temperature, which permits its association with alternative energy sources viz. geothermal, solar, and industrial residual heat; (b) operation at room pressure Subramani and Jacangelo [10], which increases air gap membrane distillation system safety and reduces equipment costs; and (c) membrane fouling is less severe [11]. Due to these characteristics, MD has recently been extensively investigated, and it is anticipated that it will ultimately emerge as a cost-effective technology for treating water and wastewater [12]. As a consequence of these characteristics, MD has recently been the subject of extensive research, and believed to be a cost-effective method of water and effluent treatment. In accordance with driving force generation and permeate collection, the membrane distillation is categorized into four types: (a) Vacuum Membrane Distillation (VMD), (b) Direct Contact Membrane Distillation (DCMD), (c) Air Gap Membrane Distillation (AGMD) and (d) Sweeping Gas Membrane Distillation (SGMD) [13,14]. Among all configurations, AGMD is the optimal configuration when a layer of stagnant air is introduced between the membrane and condensation surface. The feed evaporates at the interface of the membrane and the liquid, and the evaporated substance passes through the membrane. The liquid then travels through the air gap before condensing on the coolant plate [15]. The difference in temperature between the feed aqueous mixture and the cold surface drives the evaporation of water and the volatile component at the heated feed/membrane interface. In AGMD, similar to other membrane distillation configuration, both mass and thermal transfer occurs simultaneously through the membrane. The air gap in this configuration is advantageous

because it reduces the issue of heat loss caused by membrane conduction. Conversely, the air gap between the membrane and condensing surface provides an additional mass transfer barrier and reduces the flux of permeate [16].

Similar to other MD processes, AGMD governs with simultaneous heat and mass transfer during operation. Henceforth, in order to determine effect of process parameters such as feed bulk inlet temperature, feed concentration, membrane air gap width, and feed flow rate on permeate flux of respective migrating species and selectivity, it is important to estimate the manipulating variables namely feed side membrane surface temperature and cooling plate temperature at air gap side. These variables can be determined experimentally but not possible always. Therefore, there is a need to develop heat and mass transfer correlations for AGMD process which will be helpful in determining the permeate flux mathematically. In the literature, various authors [17-19] have made heat and mass transfer correlations for MD. But the authors Kalla et al. [20] had worked for breaking azeotrope of HCl/water using AGMD and developed the heat transfer correlation by considering the heat transfer through boundary layer by bulk flow. It is worthwhile to mention that contribution of convective flow heat transport will also take place in combination with bulk flow; the contribution of the former is neglected by the author. Therefore, the developed correlation by the author may not be accurate enough for estimating the heat transfer coefficient and finally the permeate flux. In this context, an effort has been made in the present objective to develop the heat transfer correlation by considering the contribution of bulk and convective heat transport concurrently at hot feed side of the membrane for the separation of volatile organic compound using AGMD. In this work, benzene-water mixture is considered for its separation through AGMD. Moreover, in the study [20], the heat transfer coefficient due to convective heat flux across the membrane is taken as the ratio of gas phase thermal conductivity and air gap thickness however, in actual it accounts for simultaneous heat and mass transfer in the system due to transfer of sensible heat by the diffusing vapors through the membrane from the liquid phase to vapor phase. Therefore, in this study heat transfer coefficient term under Newton's law of cooling is strengthened as additional unique objective by incorporating the sensible heat and diffusion mechanism simultaneously. The empirical heat transfer correlation at hot feed side is developed in terms of dimensionless number i.e., Nusselt number (Nu) relating other dimensionless numbers namely Prandtl number (Pr) and Reynolds number (Re) using Newton's method by minimizing sum of square errors. In similar manner, mass transfer correlation for Schmidt number (Sc) was developed with respect to Sherwood number (Sh) and Reynolds number (Re). The membrane morphology and pore size distribution, before and after the experiment were also studied through FE-SEM and AFM images qualitatively and quantitatively for investigating the fouling phenomena during experiment.

2. Experimental

2.1 Materials required

Millipore manufactured poly-tetra-fluoro-ethylene (PTFE) hydrophobic membrane with nominal pore size of 0.22 μm was used for AGMD experiments. The outline of the membrane characteristics is given in Table 1. Deionised Water was obtained in the laboratory employing conventional distillation apparatus and certified reagent A.C.S. grade benzene (>99.0%, EMPLURA) (acquired from Abhishek Chemicals Co., Ltd., Jaipur).

Table 1. Membrane Characteristics

Properties	Range
Module Diameter (mm)	90
Hydraulic Diameter (D_h) (mm)	45
Material	PTFE
Porosity (%)	85
Thickness (µm)	150
Pore Size (diameter) (µm)	0.22
Manufacturer	Millipore

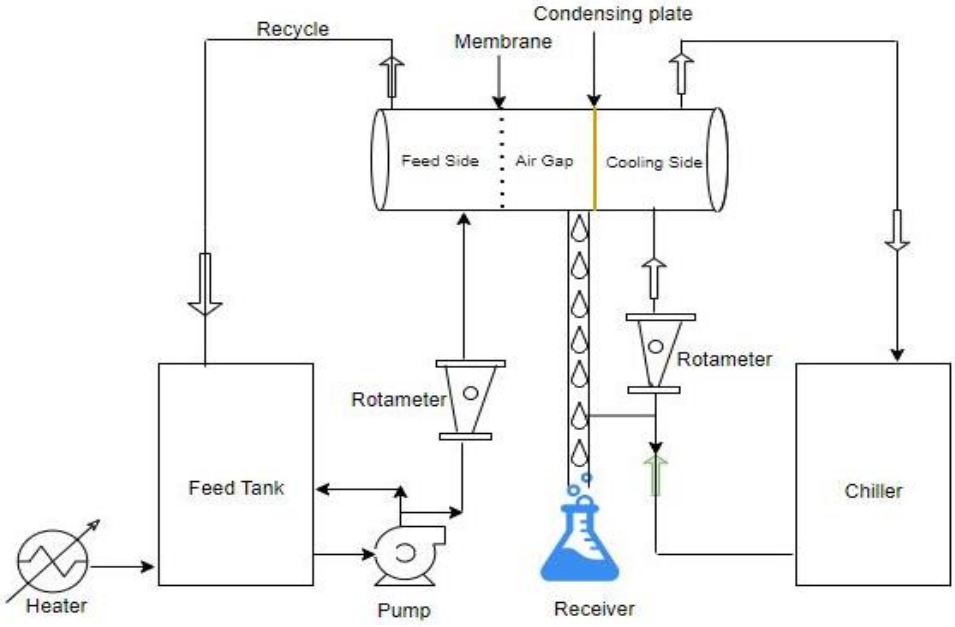

Figure 1. Schematic diagram of air gap membrane distillation set-up

2.2 Experimentation

A fabricated AGMD lab-scale set-up was used in this study for separating the aqueous solution of benzene-water system. The membrane module of AGMD experimental set-up comprises of 4 sections namely, the hot feed section, the membrane section, the air gap section, and the refrigeration section respectively. The schematic diagram of AGMD set up and its membrane module with its dimensions are illustrated in Fig. 1-2, respectively. In this work, the feed solution of 1000 mg/l benzene was circulated using pump from the feed tank (capacity 20 liters) to the hot feed side of the membrane module, while the retentate was rejected separately. The temperature controller heater is connected to the feed reservoir so that the feed solution can be heated to the desired temperature. The Type-J thermocouple was utilized, in order to get an accurate reading of the feed mixture. From the chiller, cooling water was circulated continuously to the refrigeration side of the membrane module. Using rotameters (Starflow, India), the volumetric velocity of hot

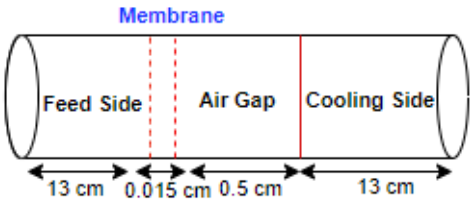

Figure 2. Dimensions of membrane module

Table 2. Specification of various Instruments used in AGMD set-up

Instrument	Specification	Manufacturer
Feed Pump	Capacity: 10 L/min Head: 3-4 meter Motor: 0.5 HP, 2900 RPM, 220 v	Leakless Pumps & Sealings Equipments, Mumbai, India
Cooling Pump	Capacity: 10 L/min Head: 3-4 meter Motor: 0.5 HP	Prasad Overseas, Jaipur, India
Chiller	Capacity: 50 L, Operating temperature: -15 to 20°C	M/s LABROS INSTRUMENTS, Jaipur
Rotameter	Range: 1- 10 liter/min	Starflow, India
Thermocouple	Type J Digital Thermocouples, PT-100	Techno Instruments, Gujarat

feed mixture and cooling water were monitored. The benzene and water vapors migrate across the hydrophobic membrane section from the feed side and get condensed on the cooling plate of the air gap section of the membrane module and finally collected in the receiver. The permeate concentration of benzene was found using UV-Vis spectrophotometer at wavelength of 255 nm. The membrane surface morphology was characterized using FE-SEM, EDS, and AFM. The specifications and manufacturer of the equipment/ instruments are detailed in Table 2. The liquid entry pressure (LEP) for PTFE membrane was estimated to be 3.1 bar using $LEP = -2\gamma \cos\theta / r_{max}$ where γ is surface tension of the liquid (0.0662 N/m at 60 °C), θ is contact angle of membrane (118°), r_{max} is maximum pore radius of membrane (0.2 μm).

3. Results and discussions

3.1 Heat transfer correlation

In AGMD, both mass and heat transfer occur simultaneously. Consequently, heat transfer coefficient (HTC) and mass transfer coefficient (MTC) has a significant role in permeate flux. In AGMD, volatile component at the feed side vaporizes and creates vapor-liquid interface at the hydrophobic membrane surface. These vapors penetrate across the membrane matrix and get condensed in the air gap on the vertical condensing plate [21]. During component mass transfer across zones from feed side to air gap, the simultaneous heat transfer will also take place as represented in Fig. 3. Various heat transfer correlations are available in the literature but mostly are valid for non-porous and rigid heat exchangers [22]. However, in this study, the membrane is

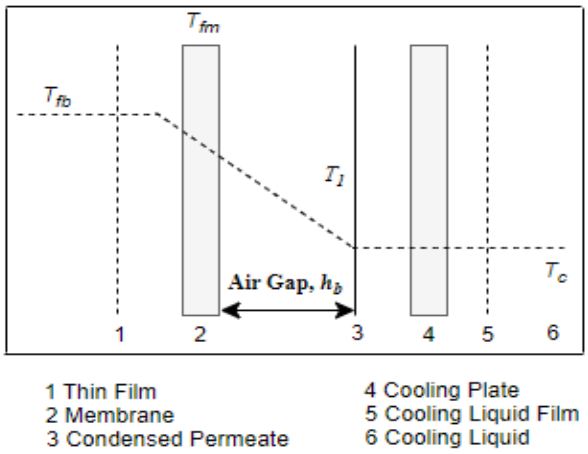

Figure. 3 Schematic heat transfer profile of AGMD process

porous in nature; there is difference between the processes of heat transfer in AGMD as compared to heat exchanger. Moreover, the former is also coupled with mass transfer. Therefore, the empirical correlation available for heat exchangers cannot be used directly for AGMD process. Hence, in this present study, the simultaneous heat and mass transfer phenomena were considered in order to obtain the heat transfer correlation in terms of Nusselt No. (*Nu*), Reynolds No. (*Re*), and Prandtl number (*Pr*).

The heat energy required for the evaporation of the species (benzene-water) at the liquid-membrane interface into the membrane pores is provided by the heat supplied from the bulk solution. The heat flux (q_h) from the solution to the membrane surface is the combination of heat transfer through the boundary layer by bulk flow and convective flow as follows [23].

$$q_h = \underbrace{h_{hft}(T_{fb} - T_{fm})}_{\text{Bulk Flow}} + \underbrace{\sum_{i=1}^{2} N_i C_{pli} (T_{fb} - T_{fm})}_{\text{Convective Flow}} \tag{1}$$

Where, h_{hft} is the liquid film heat transfer coefficient at hot feed side in W/m^{2}K, C_{pli} is the specific heat of mixture component in liquid feed at $\left(\frac{T_{fb}+T_{fm}}{2}\right)$ in J/kg.K , T_{fb} and T_{fm} are the hot feed side temperature and membrane surface temperature at feed side respectively as indicated in Fig. 3. In the Eq. (1), N_i is the flux of transferring species *i* in kg/m^2 h.

The total transfer of heat (q_a) from liquid-phase (membrane side) to the vapor-phase (cooling plate) in the AGMD module takes place via convective heat flux (Q_c) in air gap and due to latent heat of vaporization (Q_H).

$$q_a = Q_c + Q_H \tag{2}$$

$$\Rightarrow q_a = h'(T_{fm} - T_1) + \sum_{i=1}^{2} N_i H_i \tag{3}$$

Where, T_1, N_i, H_i, and h' are the condensate temperature (K) on the cooling plate in the air gap, the permeate flux of species (kg/m^{2}h), the latent heat of vaporization (J/kg), the heat transfer coefficient (W/m^{2}K). The connective heat flux (Q_c) is considered and represented in Eq. (3) using Newton's law of cooling in which the Ackerman correction factor is accounted in the term h'due to simultaneous heat and mass transfer in the system and $h^{'}$ is considered as follows [24].

$$h^{'} = h_b\theta = \frac{h_b\left(\frac{\sum_{i=1}^{2} N_i C_{pgi}}{h_b}\right)}{\left(1 - e^{-\frac{\left(\sum_{i=1}^{2} N_i C_{pgi}\right)}{h_b}}\right)} \tag{4}$$

The Ackerman correction factor θ seen in the Eq. (4) expresses the effect of mass transfer on the value of heat transfer coefficient since it accounts for sensible heat getting transferred by the vapors during diffusion process across the membrane. The value of Ackerman correction factor (θ) is defined as follows [24].

$$\theta = \frac{\left\{\frac{\left(\sum_{i=1}^{2} N_i C_{pgi}\right)}{h_b}\right\}}{1 - exp\left\{-\frac{\left(\sum_{i=1}^{2} N_i C_{pgi}\right)}{h_b}\right\}} \tag{5}$$

where, h_b is the heat transfer coefficient (W/m^{2}K), which being related to all the components present in the mixture. Mathematically, it is the ratio of k_m/δ wherein k_m and δ is the vapor phase mixture thermal conductivity in (W/m.K), and air gap (m) respectively. The mixture thermal conductivity of the vapor phase k_m is estimated using the following Eq. (6) [25].

$$k_m = 0.5\,\frac{k_A k_B}{x_A k_B + x_B k_A} + 0.5\,(k_A x_A + k_B x_B) \tag{6}$$

Where, k_A and k_B are the respective thermal conductivities of benzene and water (W/m.K). In addition, x_A and x_B represent the mole fractions of benzene and water in the vapor phase, respectively.

The heat flux at the surface of the condensate at the cooling plate is represented by Eq. (7) as follows:

$$q_c = h_c(T_1 - T_c) \tag{7}$$

Where, h_c is the overall heat transfer coefficient due to condensate film, thickness of the cooling plate, and coolant film at the cooling side and T_c is the temperature of the condensate film.

Under steady state heat transfer, the heat flux is constant across the transportation stages in MD:

$$\begin{gathered} \frac{dq}{dz} = 0 \\ \Rightarrow q_h = q_a = q_c \\ \Rightarrow h_{hft}\left(T_{fb} - T_{fm}\right) + \sum N_i C_{pli}\left(T_{fb} - T_{fm}\right) = h^{'}\left(T_{fm} - T_1\right) + \sum N_i H_i \end{gathered} \tag{8}$$

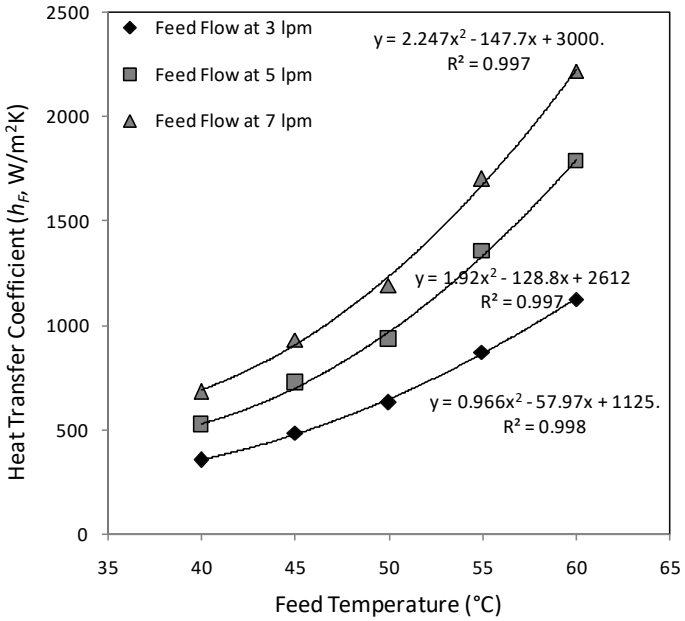

Figure. 4 Effect of hot side feed temperature on heat transfer coefficient [Air gap thickness = 3mm, Benzene concentration in feed =1000 mg/l, cooling plate temperature = 10° C]

The Eq. (8) can be rewritten as:

$$h_F\left(T_{fb} - T_{fm}\right) = h'\left(T_{fm} - T_1\right) + \sum N_i H_i \tag{9}$$

Where, $h_F = h_{hft} + \sum N_i C_{pli}$ is the combined heat transfer coefficient (W/m^{2}K) at hot feed side due to convective and bulk flow.

The hot feed side heat transfer coefficient h_F was calculated from Eq. (9) at various hot feed temperatures and feed flow rate. The N_i, T_{fm}, and T_1 were measured experimentally whereas latent heat of vaporization (H_i) is considered at the average temperature of the hot feed side $\frac{T_{fb}+T_{fm}}{2}$. The values of specific heat (C_{pgi}) for benzene and water vapor were taken at $\frac{T_{fm}+T_1}{2}$ (arithmetic average of membrane surface temperature and condensing film surface temperature). After estimating all the physical quantities under various conditions along with permeate flux, the combined heat transfer coefficient is estimated. From Fig. 4, it was found that the combined heat transfer coefficient at hot feed side increased from 350.73 to 1123.06, 523.27 to 1786.36, and 679.24 to 2219.14 W/m^{2}K on increasing the hot feed side temperature from 40 to 60°C at 3, 5, and 7 lpm of hot feed side flow rate respectively under constant air gap width of 3 mm and 1000 mg/l feed concentration of benzene. This can be attributed by the fact that on increasing the hot feed side temperature, the fluid feed viscosity (μ) decreases which leads to increase in the heat transfer coefficient since, heat transfer coefficient is related to fluid viscosity as$h_f \propto \mu^{-0.5}$. Moreover, on increasing the hot feed side temperature, the temperature polarization will get decreased resulting in decline of the thermal boundary layer thereby increase the heat transfer coefficient [26].

A correlations between combined heat transfer coefficient and hot feed temperature was developed under various feed flow rate using minimization of squares of error as follows:

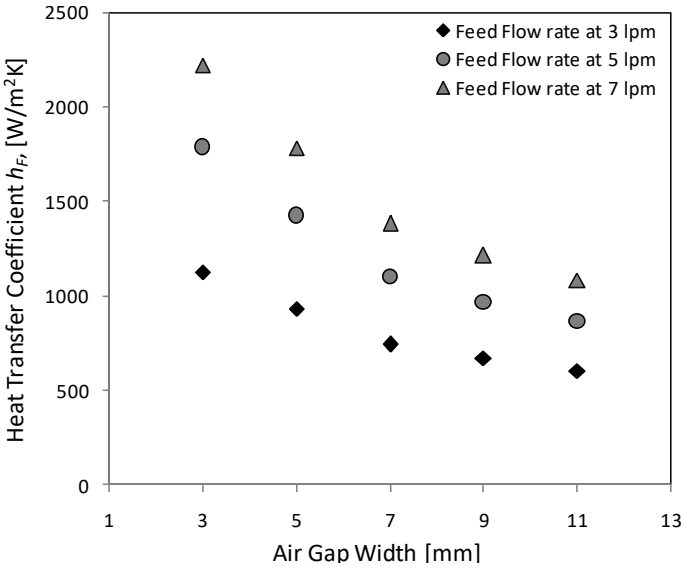

Figure. 5 Effect of Air gap thickness of benzene-water on heat transfer coefficient [Hot Feed Temperature = 60°C, Benzene Concentration in feed = 1000 mg/l, cooling plate temperature = 10° C]

$$\text{At 3lpm, } h_F = 0.966\, T_{fb}^2 - 57.97\, T_{fb} + 1125 \tag{10}$$

$$\text{At 5 lpm, } h_F = 1.92\, T_{fb}^2 - 128.8\, T_{fb} + 2612 \tag{11}$$

$$\text{At 7lpm, } h_F = 2.247\, T_{fb}^2 - 147.7\, T_{fb} + 3000 \tag{12}$$

The R^2 values for the aforementioned equations were estimated to be 0.998, 0.997, and 0.997, respectively for 3, 5, 7 lpm of feed flow rate, which represent the close proximity between experimental values and fitted non-linear model. This non-linear behavior between heat transfer coefficient and hot feed temperature is due to the reason that vapor pressure of component and temperature is related exponentially by Antoine equation [27].

Air gap is one of the predominant parameter affecting the performance in AGMD process therefore; this study is extended to investigate the effect of air gap on heat transfer coefficient. It is evident from the Fig. 5, that the heat transfer coefficient decreased from 1123.10 to 603.78, 1786.36 to 864.68, 2219.14 to 1083.51 W/m^{2}K on increasing the air gap width from 3 to 11 mm at different feed flow rates of 3, 5, and 7 lpm respectively under constant hot feed side temperature of 60°C and feed benzene concentration of 1000 mg/l. The reason for this decrement may be attributed by the fact that on increasing the air gap width, the mass transfer resistance increases which causes a decrease in the thermal water bridging effect resulting in reduction of the heat flow across the junction thereby heat transfer coefficient (h_F) decreases [28].

The Nusselt Number (*Nu*), Reynolds Number (*Re*), and Prandtl Number (*Pr*) for hot feed side are estimated using the standard formula [29].

$$Nu = \frac{h_F D_h}{k_{ml}} \tag{13}$$

$$Re = \frac{\nu\, D_h \rho_{ml}}{\mu_{ml}} \tag{14}$$

$$Pr = \frac{\mu_{ml} C_{plm}}{k_{ml}} \tag{15}$$

where, D_h, k_{ml}, ν, ρ_{ml} , μ_{ml} , C_{plm} are the hydraulic diameter of the membrane (m), hot feed side benzene-water mixture thermal conductivity (W/m.K) in liquid phase, feed liquid approach velocity (m/s), feed liquid mixture density (kg/m^3), mixture viscosity (Pa.s), and mixture specific heat (J/kg.K) in liquid phase at feed side.

The physical values for liquid phase mixture at hot feed side were estimated using following mixture rules [30-32].

$$k_{ml} = \lambda_1 x_1^2 + \lambda_2 x_2^2 + 2\lambda_{12} x_1 x_2 \tag{16}$$

$$\rho_{ml} = \frac{1}{\frac{x_1}{\rho_1} + \frac{x_2}{\rho_2}} \tag{17}$$

$$\mu_{ml} = (x_1 \times \mu_1^{0.33} + x_2 \times \mu_2^{0.33})^{0.33} \tag{18}$$

$$C_{plm} = x_1 C_{p1} + x_2 C_{p2} \tag{19}$$

where, λ_1, λ_2 , x_1, x_2, ρ_1, ρ_2, μ_1, μ_2, C_{p1} and C_{p2} are the thermal conductivity (W/m.K), mole fraction, density (kg/m^3), viscosity (Pa.s), specific heat (J/kg.K). The subscript '1' and '2' denote benzene and water, respectively. The following non-linear empirical heat transfer correlation was considered relating *Nu* with other dimensionless numbers, namely Reynolds and Prandtl numbers that affect the heat transfer in the boundary layer at hot feed side:

$$Nu = a\, Re^b\, Pr^c \tag{20}$$

where, *a*, *b* and *c* are the characteristics constant which depends upon the AGMD module design and polarization effect, and the membrane characteristics. The proposed non-linear model was fitted by minimising the square of the error between experimental and estimated values using Newton's method. After the regression analysis, the optimum values of *a*, *b*, and *c* were obtained to be 0.08, 1.15, and 0.33, whereas the empirical correlation is established as follows:

$$Nu = 0.08\, Re^{1.15}\, S\, c^{0.33} \tag{21}$$

The theoretical and experimental plot between log ($Nu/Pr^{0.33}$) and log (*Re*) is represented in Fig. 6. It is evident from the figure that the developed theoretical model is in good agreement with the experimental data since the R^2 value was found to be 0.982.

3.2 Mass transfer correlation development

In AGMD process, both heat and mass transfer occur simultaneously. The migration of vapors from feed-side through the hydrophobic porous membrane causes mass transfer, which relies on the flow rate, hot-side feed temperature. Therefore, in order to investigate the process precisely, it is important to determine the mass transfer coefficient and correlation, which will be helpful in understanding boundary layer phenomena, designing and controlling the process. Henceforth, in

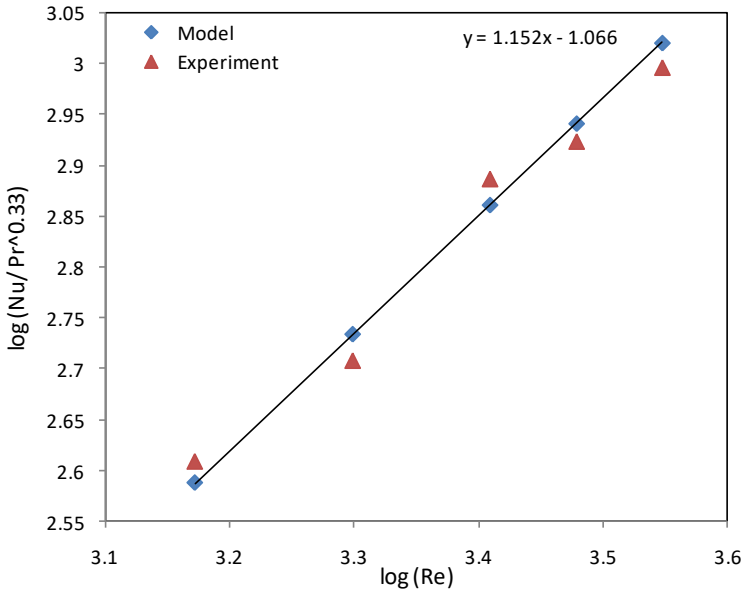

Figure. 6 Heat transfer correlation fitting curve

this study, upon estimation of mass transfer coefficient (k_f), the mass transfer correlation was established in terms of the Sherwood number (*Sh*), as a function of dimensionless numbers like Schmidt (*Sc*) and Reynolds number (*Re*) as follows [33].

$$Sh = e\,Re^{f}\,S\,c^{g} \tag{22}$$

where, $Sh = k_f D_h/D_{AB}$, $Sc = \mu/\rho D_{AB}$, D_{AB} is the diffusivity of components with respect to air at different temperatures. μ and ρ are the densities and viscosities of migrating components (benzene and water) across the membrane, k_f is the mass transfer coefficient, and D_h is the hydraulic diameter. The individual mass transfer (k_{fi}) of benzene and water was estimated by the following Eq. (23) [20].

$$k_{fi} = \frac{N_i R \Delta T}{M_i\left(P_{mfi} - P_{pgi}\right)} \tag{23}$$

where, M_i (molecular weight) of individual component, P_{mfi} (vapor pressure) at the membrane side, P_{pgi} (vapor pressure) on permeate side (cooling plate). N_i is component permeate flux, R is universal gas constant (mmHg) and ΔT is the difference between the membrane temperature and cooling temperature.

The mass transfer coefficient was calculated using Eq. (23) at various hot feed temperatures (40-60°C), feed flow rate 3-7 lpm under constant feed benzene concentration of 1000 mg/l and air gap width of 3 mm. It is observed from the Fig. 7 that on increasing the hot feed side temperature from 40°C to 60°C, the mass transfer coefficient of water (k_{fw}) increased from 9.64×10^{-2} to 1.83×10^{-1}, 1.08×10^{-1} to 1.99×10^{-1} and 1.14×10^{-1} to 2.05×10^{-1} cm/s at 3 lpm, 5 lpm and 7 lpm respectively under constant 3 mm air gap width. Similarly, the mass transfer coefficient for benzene (k_{fb}) increased from 7.92×10^{-3} to 1.90×10^{-2}, 8.93×10^{-3} to 2.09×10^{-2}, and 9.57×10^{-3} to 2.18×10^{-2} cm/s on increasing the temperature under the same operating conditions. The reason of

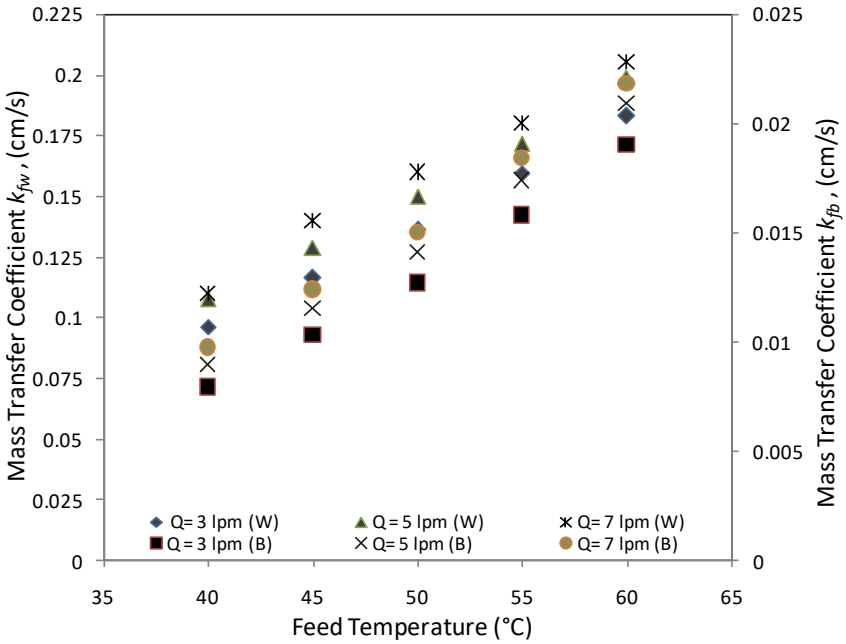

Figure. 7 Effect of feed flow rate on mass transfer coefficient [Feed Concentration= 1000 mg/l, Air Gap Width = 3mm, cooling plate temperature = 10° C]

this increment can be understood on the basis of film theory postulated by Nernst that mass transfer coefficients for different migrating species are directly proportional to the diffusivity of components wherein the diffusivity of the gases is related to $T^{3/2}$ as per the kinetic theory of the gases [34]. It was also depicted that the mass transfer coefficient of benzene is lower as compared to water. The probable reason for this can be attributed by the reason that diffusivity of benzene vapor in air (1.41×10^{-5} m^2/s at 40°C), which is approximately half than that of diffusivity of water vapor in air (2.90×10^{-5} m^2/s).

Using Newton's method, the mass transfer correlations for benzene and water were developed by minimizing the square of error between the experimental and estimated Sherwood number as follows:

$$Benzene: Sh = 2\,Re^{0.03}\,S\,c^{0.33} \tag{24}$$

$$Water: Sh = 0.5\,Re^{0.32}\,S\,c^{0.33} \tag{25}$$

The plot between log ($Sh/Sc^{0.33}$) versus log (Re) was shown for water and benzene through Fig. 8(a)-(b). It is evident from the plot that experimental and model values are in well agreement since R^2 values ranges 0.985 to 0.976.

4. Membrane fouling

The feed benzene concentration of 1000 mg/l was fed continuously at a feed flow rate of 3 lpm in AGMD set up. The transmembrane permeate flux was collected till 420 hr. It was found

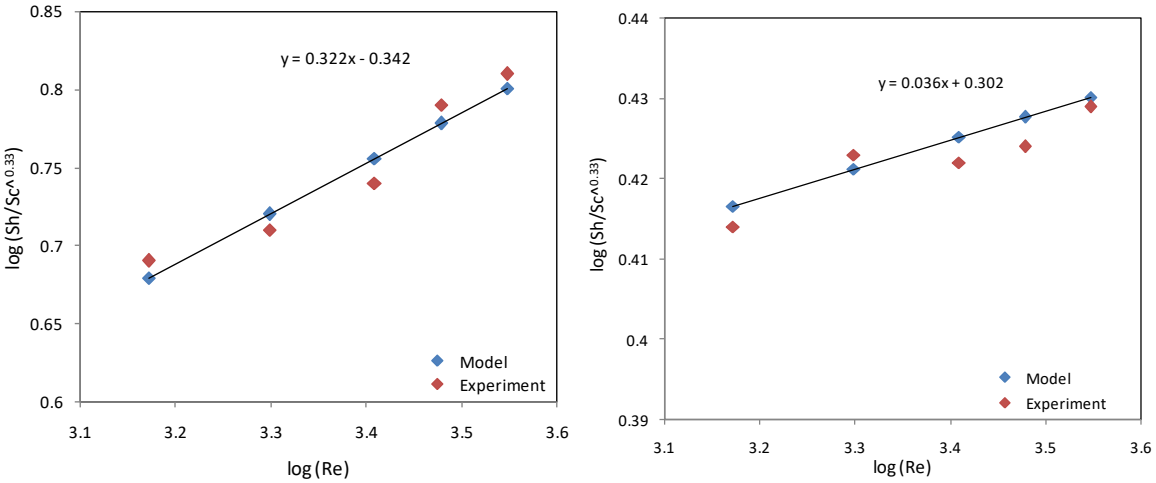

(a) (b)

Figure. 8 Mass transfer coefficient fitting curve (a) Water and (b) Benzene

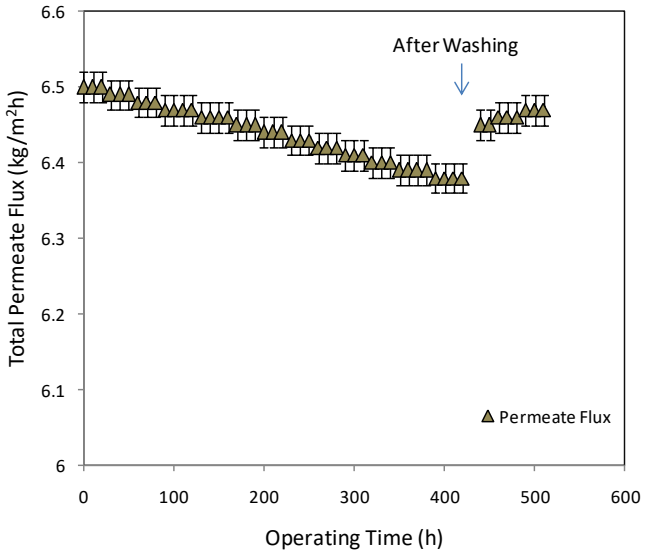

Figure. 9 Influence of operating time (h) on the total permeate flux

relatively small decline in permeate flux, as depicted in Fig. 9. Initially, the permeate flux was estimated 6.50 kg/m^{2}h at 55°C under 3 mm of gap thickness. The flux got decreased to 1.84% till 420 hr. This shows that fouling is not remarkable on the membrane surface. However, this slight decrement in flux may due to organic fouling. Moreover, the permeate flux improves after water wash and found to be 6.47 kg/m^{2}h. The fouling phenomena study is extended qualitatively and quantitatively in order to examine the membrane morphology and pore size distribution, respectively, of the fresh, used membrane after 420 h, and after water wash. It can be depicted from FE-SEM images represented in Figs. 10-12 that membrane morphologies in all three cases are nearly the same, and the fouling effect is not observed on the surface to an appreciable extent.

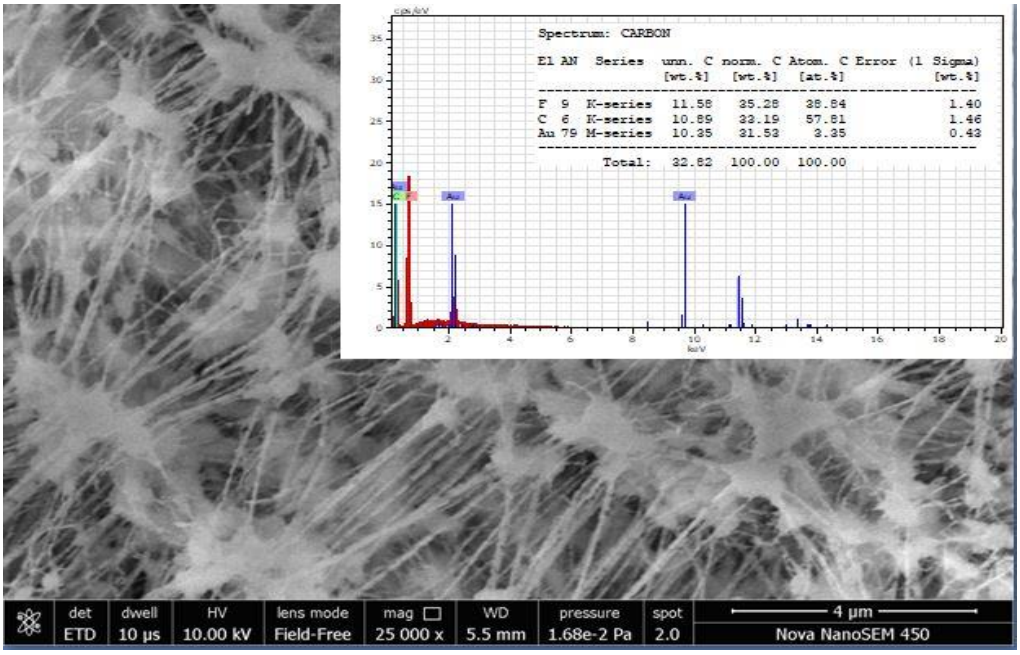

Figure. 10 FE-SEM and EDS of PTFE Fresh membrane

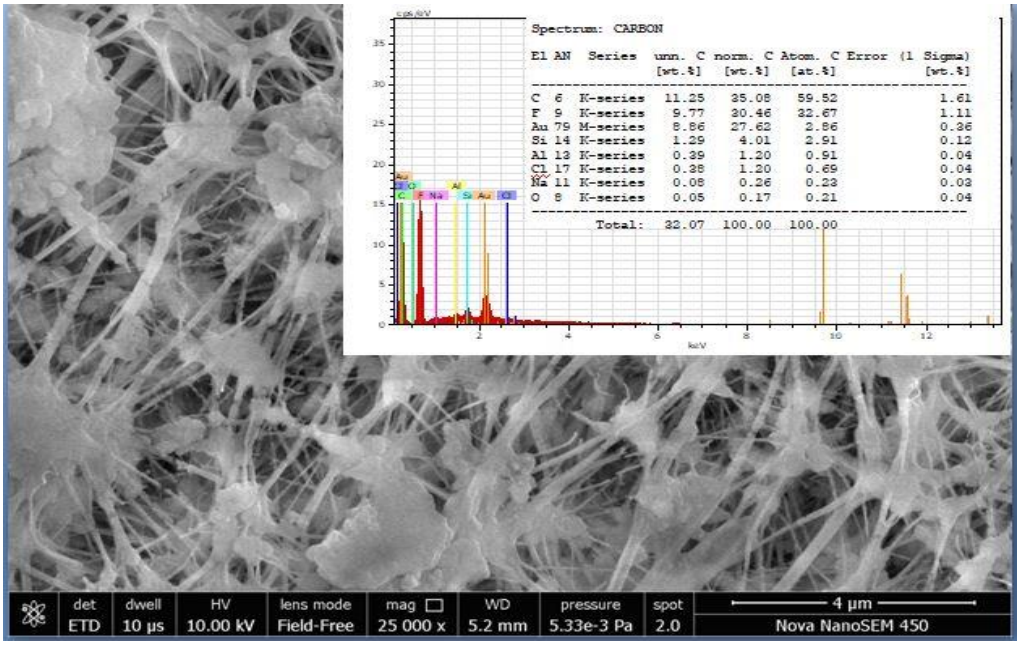

Figure. 11 FE-SEM and EDS of PTFE membrane till continuous run of 420 hr

Furthermore, pore size distribution is plotted using ImageJ software and represented in Fig. 13. The estimated area acquired through image processing was used to calculate the equivalent diameter of the membrane pores. The circular assumption was made for the pores, and the

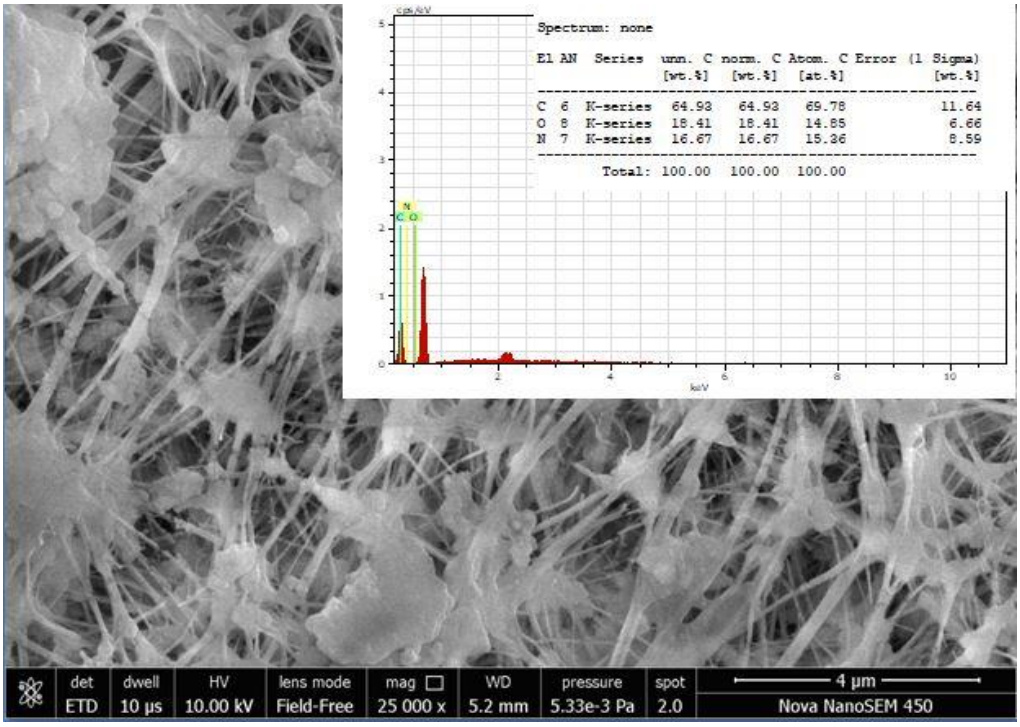

Figure. 12 FE-SEM and EDS of PTFE membrane after water wash

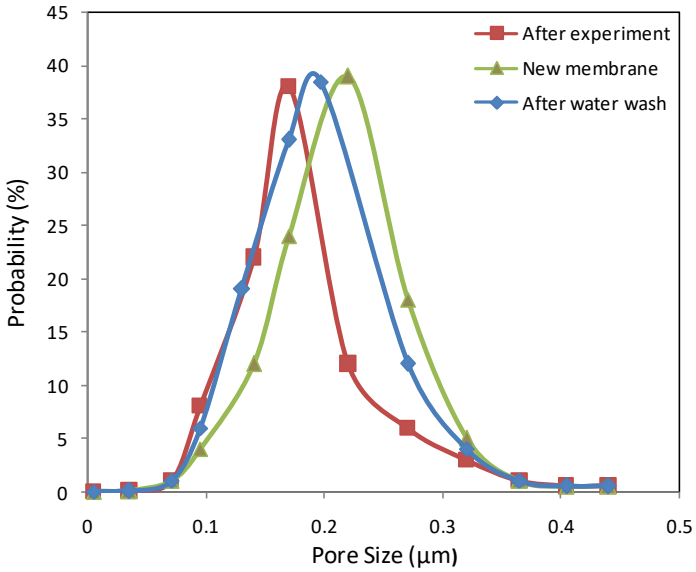

Figure. 13 Results of pore size distribution for new membrane, after 420 hr and after water wash

calculation was performed using the formula presented in Eq. (26). The average pore size of new brand membrane, used membrane till 420 h, and after water wash were found to be 0.22 micron, 0.18 micron and 0.20 micron. This difference in pore size clearly endorsed the reason for the slight

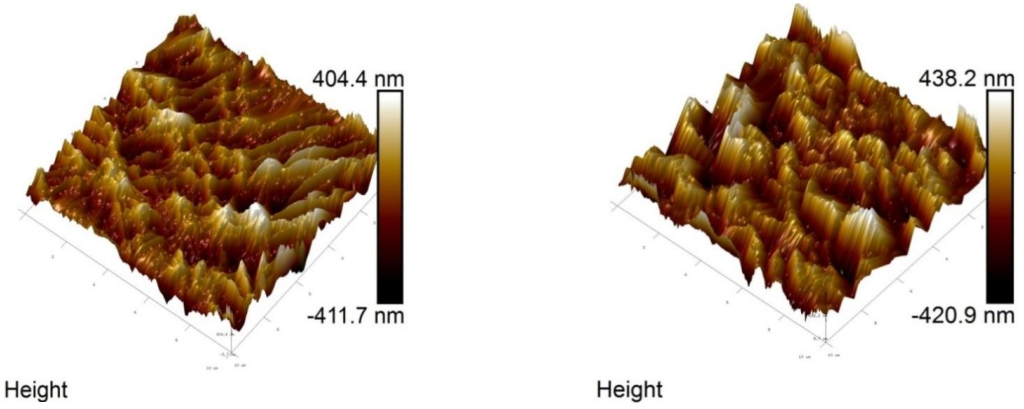

(a) (b)

Figure. 14 AFM results (a) Fresh hydrophobic PTFE membrane; (b) till continuous run of 420 hr

decrement in permeate flux and can be attributed that both the constituents in the feed are volatile in nature and hence easily penetrate across the membrane without affecting the surface properties.

The equivalent diameter of membrane pore is calculated using the Eq. (26) [35].

$$d_{eq} = 2\sqrt{Area/\pi} \tag{26}$$

However, this justification is further verified by capturing AFM images for fresh and used membrane for identifying the difference in the surface roughness quantitatively. From the AFM topographical images as shown in Fig. 14(a)-(b), for new and used membrane, it was observed that surface roughness of both membranes are similar and found to be in the range 404.4 to 438.2 nm. Also, the peaks resembles that membrane hydrophobicity is not altered to an extent thereby the flux is approximately constant throughout. This shows potential in AGMD for separation of benzene and other volatile compounds.

5. Conclusions

- In this study, AGMD process was adopted for the separation of benzene-water mixture and its performance was analyzed on the basis of total, individual permeate flux, and fouling effect.
- Heat and mass transfer correlations were developed for the hot feed side region of the AGMD system using Newton's method by minimizing the square of errors. It was observed that theoretical models are in good agreement with experimental data during correlation development.
- Four operating parameters, namely feed flow rate (3-7 lpm), air gap (3-11mm), feed temperature (40-60°C) and benzene concentration (1000mg/l) are considered in developing the correlations. It was found that the feed-side combined heat transfer coefficient increases from 523.27 to 1786.36 W/m2K on increasing the hot feed side temperature from 40 to 60°C at a feed flow rate of 5 lpm under 1000 mg/l of feed benzene concentration and 3 mm air gap width. However, the antagonistic effect of air gap width on the combined heat transfer coefficient is observed in this study. This clearly indicates that air gap width is one of the most influential parameters in the AGMD process, and hence, the tradeoff between hot feed side temperature and air gap may play a vital role in improving the separation efficiency and performance in terms of

permeate flux.

- During mass transfer correlation development, it was found that on increasing the feed flow rate, the mass transfer coefficient increases for both components (benzene and water), however mass transfer coefficient was estimated to be lower for benzene as compared to water.
- The fouling phenomena was studied quantitatively and qualitatively to examine the membrane performance and it was observed that minimal fouling was encountered on the membrane surface after a continual run of 420 h since a reduction in permeate flux was found to be from 6.50 to 6.38 kg/m2h. Moreover, after the washing, the flux retained approximately its original value.
- Fouling study was extended to verify these results using field emission scanning electron microscopy (FE-SEM), and atomic force microscopy (AFM). The pore size distribution confirms the finding of fouling phenomena. Overall, it can be concluded that AGMD has potential for effective separation of benzene-water mixture and other organic compounds.

Acknowledgement

This section is optional. Authors may acknowledge funding sources or individuals who contributed to the work.

References

1. Ahsan, A., Erabee, I.K., Nazrul, F.B., Imteaz, M., El-Sergany, M.M., Shams, S., Shafiquzzaman, M. (2023). Adsorption process efficiency of activated carbon from date pits in removing pollutants from dye wastewater. Membrane and Water Treatment, 14(4), 163-173. https://doi.org/10.12989/mwt.2023.14.4.163
2. D'Odorico, P., Chiarelli, D.D., Rosa, L., Bini, A., Zilberman, D., Rulli, M.C. (2020). The global value of water in agriculture. Proceedings of the national academy of sciences, 117(36), 21985-21993. https://doi.org/10.1073/pnas.2005835117
3. Santhosh, C., Velmurugan, V., Jacob, G., Jeong, S.K., Grace, A.N., Bhatnagar, A. (2016). Role of nanomaterials in water treatment applications: A review. Chemical Engineering Journal, 306, 1116-1137. https://doi.org/10.1016/j.cej.2016.08.053
4. Abdel-Karim, A., Leaper, S., Skuse, C., Zaragoza, G., Gryta, M., Gorgojo, P. (2021). Membrane cleaning and pretreatments in membrane distillation – a review. Chemical Engineering Journal, 422, 129696. https://doi.org/10.1016/j.cej.2021.129696
5. Ungureanu, N., Vlăduț, V., Voicu, G. (2020). Water Scarcity and Wastewater Reuse in Crop Irrigation. Sustainability, 12(21), 9055. https://doi.org/10.3390/su12219055
6. Ramos, R.L., Martins, M.F., Lebron, Y.A.R., Moreira, V.R., Reis, B.G., Grossi, L.B., Amaral, M.C.S. (2021). Membrane distillation process for phenolic compounds removal from surface water. Journal of Environmental Chemical Engineering, 9(4), 105588. https://doi.org/10.1016/j.jece.2021.105588
7. Szarka, A., Mihová, V., Horváth, G., Hrouzková, S. (2022). Development of an advanced inspection of the degradation of volatile organic compounds in electrochemical water treatment of paint-industrial water effluents. Applied Sciences, 13(1), 443. https://doi.org/10.3390/app13010443
8. Behnami, A., Zoroufchi Benis, K., Shakerkhatibi, M., Derafshi, S., Chavoshbashi, M.M. (2019). A systematic approach for selecting an optimal strategy for controlling VOCs emissions in a petrochemical wastewater treatment plant. Stochastic Environmental Research and Risk Assessment, 33(1), 13-29. https://doi.org/10.1007/s00477-018-1623-0

9. Obotey Ezugbe, E., Rathilal, S. (2020). Membrane Technologies in Wastewater Treatment: A Review. Membranes, 10(5), 89. https://doi.org/10.3390/membranes10050089
10. Subramani, A., Jacangelo, J.G. (2015). Emerging desalination technologies for water treatment: A critical review. Water Research, 75, 164-187. https://doi.org/10.1016/j.watres.2015.02.032
11. Yadav, M., Upadhyay, S., Singh, K., Chaturvedi, T.K., Vashishtha, M. (2022). Morphological study of synthesized PVDF membrane using different non-solvents for coagulation. Membrane and Water Treatment, 13(4), 173-181. https://doi.org/10.12989/mwt.2022.13.4.173
12. Biniaz, P., Torabi Ardekani, N., Makarem, M.A., Rahimpour, M.R. (2019). Water and Wastewater Treatment Systems by Novel Integrated Membrane Distillation (MD). ChemEngineering, 3(1), 8. https://doi.org/10.3390/chemengineering3010008
13. Zare, S., Kargari, A. (2018). Membrane Properties in Membrane Distillation. in Emerging Technologies for Sustainable Desalination Handbook, 107-156. Butterworth-Heinemann, UK
14. Julian, H., Nurgirisia, N., Qiu, G., Ting, Y.P., Wenten, I.G. (2022). Membrane distillation for wastewater treatment: Current trends, challenges and prospects of dense membrane distillation. Journal of Water Process Engineering, 46, 102615. https://doi.org/10.1016/j.jwpe.2022.102615
15. Yan, Z., Jiang, Y., Liu, L., Li, Z., Chen, X., Xia, M., Fan, G., Ding, A. (2021). Membrane Distillation for Wastewater Treatment: A Mini Review. Water, 13(24), 3480. https://doi.org/10.3390/w13243480
16. García-Fernández, L., García-Payo, C., Khayet, M. (2017). Hollow fiber membranes with different external corrugated surfaces for desalination by membrane distillation. Applied Surface Science, 416, 932-946. https://doi.org/10.1016/j.apsusc.2017.04.232
17. Qiao, Z., Wang, Z., Zhang, C., Yuan, S., Zhu, Y., Wang, J., Wang, S. (2013). PVAm–PIP/PS composite membrane with high performance for CO2/N2 separation. AIChE Journal, 59(1), 215-228. https://doi.org/10.1002/aic.13781
18. Alsalhy, Q.F., Ibrahim, S.S., Hashim, F.A. (2018). Experimental and theoretical investigation of air gap membrane distillation process for water desalination. Chemical Engineering Research and Design, 130, 95-108. https://doi.org/10.1016/j.cherd.2017.12.013
19. Upadhyaya, S., Singh, K., Chaurasia, S.P., Dohare, R.K., Agarwal, M. (2016b). Recovery and development of correlations for heat and mass transfer in vacuum membrane distillation for desalination. Desalination and Water Treatment, 57(55), 26886-26898. https://doi.org/10.1080/19443994.2016.1189245
20. Kalla, S., Upadhyaya, S., Singh, K., Baghel, R. (2019). Development of heat and mass transfer correlations and recovery calculation for HCl–water azeotropic separation using air gap membrane distillation. Chemical Papers, 73(10), 2449-2460. https://doi.org/10.1007/s11696-019-00795-w
21. González, D., Amigo, J., Suárez, F. (2017). Membrane distillation: Perspectives for sustainable and improved desalination. Renewable and Sustainable Energy Reviews, 80, 238-259. https://doi.org/10.1016/j.rser.2017.05.078
22. Upadhyaya, S., Singh, K., Chaurasia, S.P., Dohare, R.K., Agarwal, M. (2016a). Mathematical and CFD modeling of vacuum membrane distillation for desalination. Desalination and Water Treatment, 57(26), 11956-11971. https://doi.org/10.1080/19443994.2015.1048306
23. Cai, J., Yin, H., Guo, F. (2020). Transport analysis of material gap membrane distillation desalination processes. Desalination, 481, 114361. https://doi.org/10.1016/j.desal.2020.114361
24. Gužela, Š., Dzianik, F. (2022). Different forms of the correction factor used to describe simultaneous heat and mass transfer. Chemical and Biochemical Engineering Quarterly, 3. https://doi.org/10.15255/CABEQ.2022.2113
25. Udoetok, E.S. (2013). Thermal Conductivity of Binary Mixtures of Gases. Frontiers in Heat and Mass Transfer, 4(2). https://doi.org/10.5098/hmt.v4.2.3008
26. Olatunji, S.O., Camacho, L.M. (2018). Heat and mass transport in modeling membrane distillation configurations: A review. Frontiers in Energy Research, 6. https://doi.org/10.3389/fenrg.2018.00130
27. Wang, Z., Jia, Z., Li, R., Gao, Q., Gu, Z. (2022). Analysis and Experimental Study on Water Vapor Partial Pressure in the Membrane Distillation Process. Membranes, 12(8), 802. https://doi.org/10.3390/membranes12080802

28. Shahu, V.T., Thombre, S.B. (2019). Air gap membrane distillation: A review. Journal of Renewable and Sustainable Energy, 11(4). https://doi.org/10.1063/1.5063766
29. Hitsov, I., Maere, T., de Sitter, K., Dotremont, C., Nopens, I. (2015). Modelling approaches in membrane distillation: A critical review. Separation and Purification Technology, 142, 48-64. https://doi.org/10.1016/j.seppur.2014.12.026
30. Michal, S., Hana, N., Jan, K. (2017). The determination of viscosity at liquid mixtures – Comparison of approaches. 36th Meeting of Departments of Fluid Mechanics and Thermodynamics AIP Conference Proceedings, 020035. September.
31. Teja, A.S. (1983). Simple method for the calculation of heat capacities of liquid mixtures. Journal of Chemical & Engineering Data, 28(1), 83-85. https://doi.org/10.1021/je00031a025
32. Li, C.C. (1976). Thermal conductivity of liquid mixtures. AIChE Journal, 22(5), 927-930. https://doi.org/10.1002/aic.690220520
33. Ruiz Salmón, I., Janssens, R., Luis, P. (2017). Mass and heat transfer study in osmotic membrane distillation-crystallization for CO2 valorization as sodium carbonate. Separation and Purification Technology, 176, 173-183. https://doi.org/10.1016/j.seppur.2016.12.010
34. Bird, R.B., Stewart, W.E., Lightfoot, E.N. (2002). Transport Phenomena. John Wiley & Sons.
35. Phattaranawik, J. (2003). Effect of pore size distribution and air flux on mass transport in direct contact membrane distillation. Journal of Membrane Science, 215(1-2), 75-85. https://doi.org/10.1016/S0376-7388(02)00603-8